ADVANCED FUNCTIONAL MATERIALS
www.afm-journal.de

Nematic Liquid Crystals Embedded in Cubic Microlattices: Memory Effects and Bistable Pixels

Francesca Serra, Shane Michael Eaton, Roberto Cerbino, Marco Buscaglia, Giulio Cerullo, Roberto Osellame, and Tommaso Bellini*

The confinement of liquid crystals in geometries with frustrating boundary conditions gives rise to nontrivial effects such as bistability and memory. It is shown that large memory effects arise when nematic liquid crystals are embedded in cubic micrometer-sized scaffolds made by two-photon polymerization. The electric field alignment of the liquid crystals inside the porous medium is maintained when the applied field is above a threshold (approximately 2 V per micrometer of cell thickness). The onset of the memory is an on/off type process for each individual pore of the scaffold, and the memory typically starts emerging in one region of the structure and then propagates. The global memory effects in porous structures with controlled geometry are enhanced with respect to the case of random porous structures. This work is a proof of the "memory from topology" principle, which was previously suggested by computer simulations. These new materials can pave the way to new types of bistable displays.

1. Introduction

The nematic phase of thermotropic liquid crystals (NLCs) is a fluid state in which anisotropic molecules spontaneously develop long-ranged orientational order, giving rise to anisotropic mechanical, optical and dielectric properties.[1] The combination of fluidity and anisotropy is at the core of all technological exploitations of NLCs in the display industry and as light modulators. These applications also rely on the capability of controlling the coupling between NLC and solid surfaces, such as those that confine the NLCs within the displays. Various strategies have been developed to treat surfaces in order to favor the alignment of the mean molecular axis, the so-called nematic director, in a given direction parallel, oblique or perpendicular to the solid-NLC interface.[2]

Dr. F. Serra, Dr. R. Cerbino, Dr. M. Buscaglia, Prof. T. Bellini
Dipartimento di Biotecnologie Mediche e Medicina Traslazionale
Università degli Studi di Milano
Via F.lli Cervi 93, 20090 Segrate, Milano, Italy
Dr. S. M. Eaton, Prof. G. Cerullo, Dr. R. Osellame
Istituto di Fotonica e Nanotecnologie (IFN) - CNR and Dipartimento di Fisica - Politecnico di Milano
P.zza Leonardo da Vinci, 20133 Milano, Italy
E-mail: shane.eaton@ifn.cnr.it

DOI: 10.1002/adfm.201203792

Composite materials made from NLCs and micrometer-scale 3D elements are also studied for their peculiar optical and electro-optical properties. As an example, NLCs can be employed as a smart matrix to guide the assembly of microparticles in the ordered geometries needed in photonic crystals. When microparticles are introduced to the NLC, the coupling between their surfaces, adequately treated, and the nematic director produces a variety of possible distortions and topological defects, i.e., point or lines in which NLCs concentrate the elastic stress. When more microparticles are present, the distortion of the NLCs due to particles and the topological defects give rise to interparticle interactions, in turn promoting their spatial ordering, as demonstrated by numerous experiments, theory and computer simulations.[3–6]

A parallel and symmetric investigation involves the behavior of NLCs embedded in microstructured bicontinuous solid porous matrices (BSPMs) with interconnected cavities, aimed at the development of multistable materials,[7,8] capable of maintaining the *on* or *off* state of the pixels after removal of the applied field. Such an effect can be exploited in alternative energy-saving bistable displays to compete with conventional electrophoretic e-paper.[9,10] In BSPM a surface divides the space into two separate interconnected regions. When this surface favors perpendicular (homeotropic) anchoring, NLCs, which occupy one of the interconnected regions, always develop topological defects that produce torques effectively constraining the nematic director to align in given directions within the pores. Recent computer simulations of NLCs incorporated in BSPMs of various geometries and symmetries[11] showed: i) that the number, length and trajectories of topological defect lines are not uniquely determined by the solid structure and ii) that the application of sufficiently strong electric fields can significantly change the conformation of the system by disentangling defect lines from the solid structure and rewiring them along different paths. Such a field-induced topological change yields new states that do not relax to the original one.[11] According to the simulations, the strength of memory effects, measured as the variation in birefringence and optical axis direction between distinct stable states, depends on the geometry of the BSPM and is maximum in bicontinuous cubic porous networks.

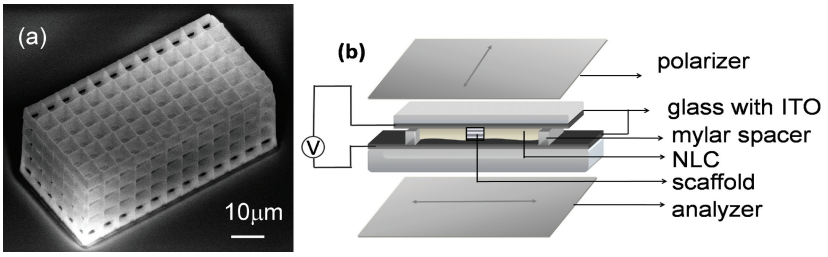

Figure 1. Fabrication of a bistable solid porous matrix: a) SEM image of a 2PP fabricated scaffold, with overall dimension $30 \times 60 \times 25$ μm^3, 5-μm line periodicity and b) schematic of electro-optical configuration. The cell is viewed between crossed polarizers and the field is applied between the ITO-coated glasses. The scaffold is laser-fabricated inside the cell.

Despite the intriguing prediction provided by the simulation work, an experimental demonstration of multistability of NLCs confined in a BSPM is still lacking, due to the difficulty of tailoring the porous materials into different controlled 3D geometries. Direct laser writing by two-photon polymerization (2PP)[12] is an ideal fabrication technique for such structures due to its high resolution and 3D patterning capability.[13–16] In this work we show the first demonstration of multistability of NLCs incorporated in BSPM having nearly cubic symmetry.

2. Results and Discussion

Micrometer-scale 3D scaffold structures were fabricated in a sandwich of two electrically conductive ITO-coated glass substrates, (top and bottom glass 160-μm and 1-mm thick, respectively), separated by 25-μm thick mylar spacers. The structures were formed by direct laser writing in a hybrid organic-inorganic photoresist (SZ2080), which offers high optical quality and good mechanical stability.[17] 3D scaffolds were formed with an average power of 12 mW and scan speed of 60 μm/s (SEM image shown in **Figure 1**a), conditions shown previously to yield uniform and mechanically stable microstructures.[18] Scaffolds were fabricated with a spacing of 5 μm between adjacent pillars (optimum size for observing the scaffold with the microscope and also to observe bistability), a height of 25 μm and total areal dimensions of either 30×60 μm^2, 50×50 μm^2 or 50×100 μm^2. These areal dimensions are comparable to the 78-μm pixel width of the currently available commercial display with the highest pixel density (Retina Display of iPhone 5), which suggests that each 3D structure could represent an individual pixel in a display.

After the fabrication of the scaffolds, copper wires were attached with conductive glue to the ITO-coated sides of the cell shown in Figure 1b. Surfaces were treated by submerging the whole cell in a silane solution to achieve the desired homeotropic alignment (perpendicular to surface) of the liquid crystals on the glass electrodes and on the 3D structure surface. The homeotropic alignment is essential to obtain the desired topological defects interacting with the solid surface. After silanization, the cells containing the structures were filled with liquid crystals in the isotropic phase (5CB), which were later cooled into the nematic phase. Once filled, the BSPM is formed by two complementary, interconnected and interweaved cubic networks, one solid and the other made of NLC. The optical properties of this heterogeneous material were studied by characterizing the samples by polarized transmission optical microscopy.

The images in **Figure 2** show the light transmitted through the sample in response to an electric field perpendicular to the cell surfaces. The reported values of intensity in the sketched graph are normalized to the transmitted intensity I_0 obtained after cooling from the isotropic into the nematic phase. The polarized transmission optical microscopy image on the left is acquired before applying the electric field to a 25-μm thick cell. As evident, the presence of the porous structure disrupts the uniform alignment of the NLC outside of the matrix. Indeed, the strong homeotropic anchoring on the polymer surfaces forces the NLC to follow the orientation of the surfaces, and hence to adopt distorted patterns of sizes matching the scaffold periodicity, with typical length-scale on the micrometer scale. The distorted pattern could potentially constitute a unique stable state, only dependent on the scaffold geometry. However, computer predictions[11] show that homeotropic alignment in BSPM could allow multiple stable NLC configurations, which can be switched by external forces. As the field is applied, the NLCs align along it, thus appearing dark in polarized microscopy (center image). For applied fields smaller than 20 V some areas remain slightly bright, while for higher voltages the whole sample appears completely dark.

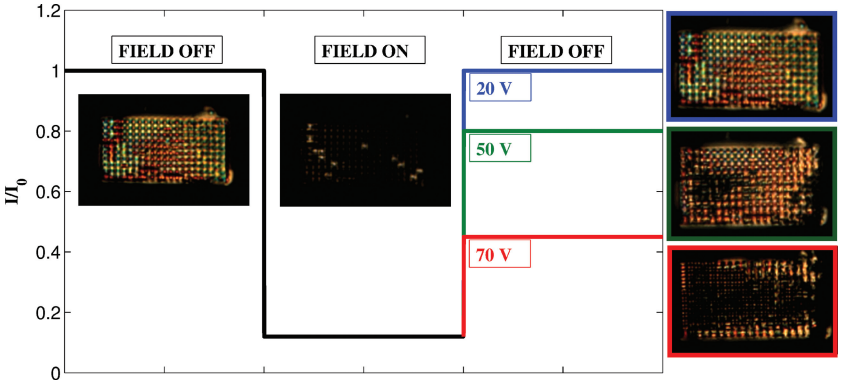

Figure 2. Memory effects in BSPMs. The overall intensity stationary values are reported. Values are normalized to the transmitted intensity I_0 measured before applying the field. The residual intensity measured after an off-on-off cycle depends on the strength of the applied field. Left inset image: sample transmission, prior to field application, showing birefringence. Here, the LCs fill the whole cell, but the intensity is non zero only inside the polymer scaffold. Outside of the scaffold, the LC alignment is perpendicular to the glass electrodes (appearing dark). Inside the scaffold, the alignment changes and follows the periodicity of the lattice. Center inset image: sample with applied field. The three images on the right show the structure transmission after the application of voltages of 20 V, 50 V, and 70 V. The structure shown in the figures has dimensions $50 \times 100 \times 25$ μm^3 and 5-μm line spacing.

After the field is removed, the liquid crystals relax to a new configuration (the three rightmost pictures), with a memory that depends on the intensity of applied field. The characteristic time of this process has not been precisely quantified yet, but the response time is always a small fraction of 1 s. After applying a 20-V voltage (Figure 2, blue), the pixel intensity reverts back to the initial bright state ($I/I_0 = 1$) showing no evidence of memory. However for a field of 50 V (green), the scaffold shows memory (I/I_0 = 0.8) of the darkened field-on state. The strongest memory was observed for voltages above 70 V (red), where, after field removal, I/I_0 = 0.45. When observed after a few days, the samples with memory were still found in the same "darker" state.

The results presented in Figure 2 are consistent with computer simulations[11] of liquid crystals in bicontinuous cubic porous materials: after the application of low fields, the NLCs elastically relax back to their initial configuration. However, when the field is large enough to break the topological defect lines, the new configuration induced by the field is stabilized by the geometry of the cubic scaffold and strong memory effects arise.

Figure 3a shows the amplitude of the memory effects obtained after removing fields of various strengths applied to the cell. In our experimental system the accessible parameter to measure the bistability is the intensity transmitted through crossed polarizers. One straightforward measurement is the mean transmitted intensity of the whole matrix. In Figure 3a this value is plotted as the remnant intensity $\Delta I = I_0 - I$ normalized to the intensity I_0 of the transmitted light before the field is applied ($\Delta I/I_0$, black curve with circles). However, this value is an average that does not differentiate between the central pores and those at the edge of the BPSM, where the alignment of the liquid crystal may be affected by border effects. Therefore, another method of quantifying the memory effect is desirable. The photos in Figure 2 suggest that the memory starts from localized regions, or groups of pores in the central part of the sample, and then expands to the whole sample. Computer simulations to reproduce this non-uniform switching are currently ongoing. Based on this observation, we adopted the different strategy of quantifying the memory as the fraction ϕ_{dark} of permanently darkened "pores", i.e., the 5 × 5-μm^2 image regions included in between adjacent pillars in the scaffold, actually corresponding to top views of columns of lattice cells. The data corresponding to this quantification of the memory effects are also reported in Figure 3a as grey squares and dashed line. Clearly, the two curves representing these two approaches have a good overlapping, although the second method seems to single out more efficiently the memory effect,

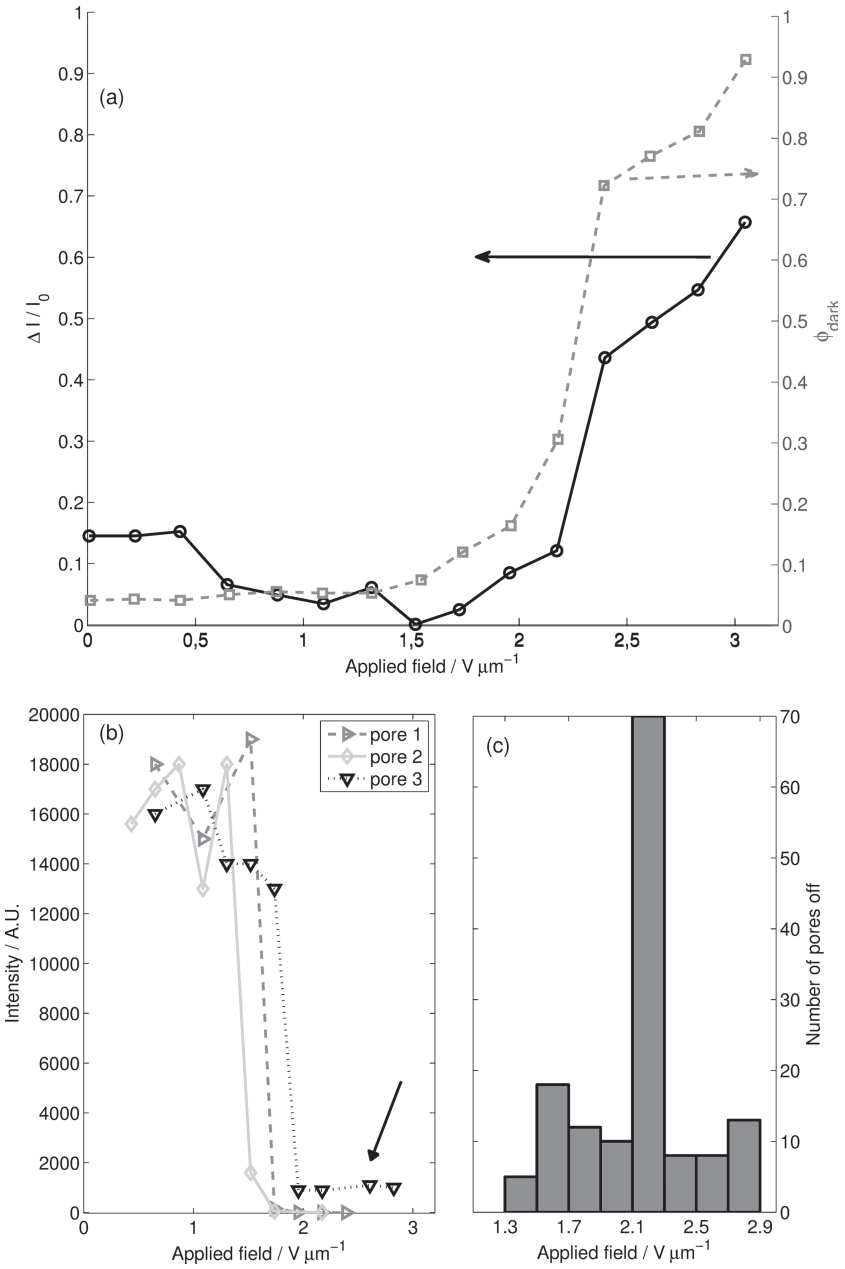

Figure 3. Dependence of the memory effects on the applied electric field, measured after the removal of the field. a) Intensity of the transmitted polarized light, after the field is switched off, is reported as a function of the applied voltage (divided by the sample thickness). The black circles on the full line represent the overall intensity variation of the structure. The grey squares on the dashed line represent the fraction ϕ_{dark} of dark pores (see the text for discussion). b) The residual intensity of a single pore after the field is switched off, measured for 3 different pores. For each pore, the intensity decreases as a step-like function. Some pores never reach a zero value of intensity (as shown by the arrow that indicates the residual intensity of the pore), and this explains why the two graphs in panel (a) do not exactly coincide. c) The highly peaked distribution of switching threshold fields for the pores. The first pores switch at fields around 1.4 V μm^{-1} but most pores switch between 2.1 and 2.3 V μm^{-1}.

which appears to have a lower value of the threshold field and a larger amplitude. The threshold voltage, divided by the thickness of the liquid crystal cell, is approximately 1.5–2 V μm^{-1}: a similar threshold was measured for the random porous matrix in previous work.[7] This value is high compared to typical electrophoretic bistable displays (about 15 V on 40-μm thickness), but comparable to the ZBD Qinetiq LC-based bistable display. Further optimization of the BPSM geometry is expected to lower the threshold field.

Following the idea that the memory starts as a local process, Figure 3b shows the brightness of a set of individual pores. We find that each pore has a step-like dependence on the field intensity, indicating that the induction of residual order is an on-off process. This observation is consistent with the onset of memory effects that depend on topological transformations: the threshold marks the necessary field strength to rewire the defect lines along topologically distinct trajectories. Such a threshold is found to change from pore to pore, likely because of the irregularity of the BSPM structure and/or because of boundary effects, as indicated by the lower value for the threshold in pores closer to the center of the sample. Boundary effects could be related to the different behavior of topological defects when closer to the edge, where less pinning sites are present. The intensity distribution of the threshold field for the switching of individual pores is shown in Figure 3c.

As already noted, although the memory effects as represented by ϕ_{dark} and $\Delta I/I_0$ behave quite similarly qualitatively, the amplitude of the memory effect is different: ϕ_{dark} approaches 1 while $\Delta I/I_0$ is always below 0.7. This difference is due not only to the already mentioned edge effects, but also to the residual birefringence that affects the dark state of the pores and that depends on the detailed geometry of the BSPM. Indeed, while ϕ_{dark} approximates the level of memory obtained by the simulations, $\Delta I/I_0$ is smaller than expected, suggesting that further optimization of the BSPM geometry may be necessary. Moreover, as also expected from the numerical simulations, ϕ_{dark} is larger than the corresponding quantity expressing the memory amplitude in random porous materials, i.e., the domain order parameter. ϕ_{dark} reaches 0.9 in the BSPM geometry, while the domain order parameter obtained from experiments on randomly interconnected porous matrices is never larger than 0.6.

The experiments reported here demonstrate for the first time the multistability of NLCs in BSPMs. The small pixel size, comparable to the commercially available pixels (Amazon Kindle Paperwhite, 120 μm; iPhone 5, 78 μm) and the response time, lower than 1 s, and comparable with other bistable displays (Amazon Kindle Paperwhite, 0.6 s), make this new type of technology interesting for possible technological applications as a LC-based bistable display.

The topological origin of the observed multistability is supported by many findings: the sharp transition in the remnant order of Figure 3b, the different behavior of pixels close to the boundaries of BSPM, the difference in memory strength between random and cubic porous geometries, and the full reversibility of memory upon melting the nematic phase and cooling back again. We note that equal BSPMs that have not been treated to provide homeotropic alignment respond to external fields in a markedly different way, with barely detectable memory effects. Further experiments focusing on the direct observation of the topological defect lines are planned.

3. Conclusions

The interaction of the liquid crystals with the confining surfaces, through the topological defects, is essential for the onset of bistability and memory. Nematic liquid crystals confined in porous media with controlled geometry exhibit large memory effects, as they retain the alignment induced by electric fields even after the field removal. Two-photon polymerization is an ideal technique to create 3D microscaffolds, with tunable size and geometry, which can be directly written in NLC cells, acting as individual pixels with bistability. Optimizing the geometry of the scaffolds is expected to further improve the performance of these bistable devices. Future work will also seek to form a larger-scale device composed of many pixels, for use as ultralow energy bistable displays.

4. Experimental Section

Direct Laser Writing of 3D Microstructures in Sandwiched Cell: 2PP was performed with a Ti:Sapphire oscillator with 87-MHz repetition rate, 40-fs pulse width, 800-nm wavelength and 400-mW average power using a 1.4-NA microscope objective (Plan-APOCHROMAT, 100× oil immersion, Zeiss). The sample was mounted on a three-axis piezoelectric motion stage (P-611.3 NanoCube, Physik Instrumente) with nanometer resolution and 100 μm × 100 μm × 100 μm travel range. The photoresist used is a hybrid organic-inorganic zirconium/silicon photoresist SZ2080, commercially available from Maria Farsari's group at FORTH in Crete, Greece. The "bis" photoinitiator 4,40-bis(diethylamino)benzophenone at a 1% concentration provides an absorption band in the UV and triggers the 2PP process. SZ2080 has high optical quality and good mechanical stability. Its low shrinkage properties make it suitable for applications sensitive to structural deformations, since additional design steps are not needed to compensate for distortions. The sandwich structure was secured with clips, filled with SZ2080 and pre-baked for 3 hours to evaporate the solvent before laser exposure. 3D scaffolds were first optimized on glass cover slips with 10 min development in a 50:50 mixture of 4-methyl-2-pentanone: isopropanol. In the sandwiched cell, the development time was significantly longer, about 20 h, since the scaffold was confined between the glass slides. Mechanically stable 3D scaffolds were formed with an average power of 12 mW and scan speed of 60 μm/s creating polymerized lines with a transversal (vertical) dimension of 1 μm (2 μm).[19]

Seeding of 3D Microstructures with Nematic Liquid Crystals: Surfaces were treated by submerging the whole cell in a silane solution (0.75 wt% dimethyloctadecyl [3-(trimethoxysilyl)propyl] ammonium chloride (DMOAP, from Sigma Aldrich) in MilliQ water), in order to achieve the desired homeotropic alignment (perpendicular to surface) of the liquid crystals both on the glass electrodes and on the 3D structure polymer surface. After silanization, the cells were filled with NLC 4-pentyl-4′-cyanobyphenyl (5CB, from Sigma Aldrich) in the isotropic phase. The filling occurred spontaneously, even after silanization, and occasional air bubbles were removed in vacuum. The sample was then observed in polarized transmission optical microscopy (PTOM) using a Nikon Optiphot 2 microscope and a Nikon D50 camera.

Acknowledgements

F.S. and S.M.E. contributed equally to the work. This project was supported by the CARIPLO Foundation (grants 2008-2413 and 2010-0635). The

authors thank Maria Farsari and Takeaki Araki for helpful suggestions. They thank Eleon Borlini for assistance with direct laser writing experiments, Matteo Salina for help with the chemical treatment of surfaces, and Alessia Turin Mangialardo and Ile Muggi Fossati for their kind help in preparing the cover design.

Received: December 21, 2012
Revised: January 25, 2013
Published online: March 13, 2013

[1] P.-G. de Gennes, J. Prost, *The Physics of Liquid Crystals*, 2nd ed., Oxford University Press, Oxford, UK **1995**.
[2] K. Takatoh, M. Sakamoto, R. Hasegawa, M. Koden, N. Itoh, M. Hasegawa, *Alignment Technologies and Applications of Liquid Crystals Devices*, 1st ed., Taylor and Francis, Abingdon, UK **2005**.
[3] J. Dontabhaktuni, M. Ravnik, Š. Žumer, *Soft Matter* **2012**, *8*, 1657.
[4] I. Muševič, M. Škarabot, U. Tkalec, M. Ravnik, Š. Žumer, *Science* **2006**, *313*, 954.
[5] M. Ravnik, M. Škarabot, Š. Žumer, U. Tkalec, I. Poberaj, D. Babič, N. Osterman, I. Muševič, *Phys. Rev. Lett.* **2007**, *99*, 247801.
[6] B. Senyuk, Q. Liu, S. He, R. D. Kamien, R. B. Kusner, T. C. Lubensky, I. I. Smalyukh, *Nature* **2013**, *493*, 200.
[7] M. Buscaglia, T. Bellini, C. Chiccoli, F. Mantegazza, P. Pasini, M. Rotunno, C. Zannoni, *Phys. Rev. E* **2006**, *74*, 011706.
[8] F. Serra, K. C. Vishnubhatla, M. Buscaglia, R. Cerbino, R. Osellame, G. Cerullo, T. Bellini, *Soft Matter* **2011**, *7*, 10945.
[9] C. Hilsum, *Philos. Trans. R. Soc. A- Math. Phys. Eng. Sci.* **2010**, *368*, 1027.
[10] B. Comiskey, J. D. Albert, H. Yoshizawa, J. Jacobsen, *Nature* **1998**, *394*, 253.
[11] T. Araki, M. Buscaglia, T. Bellini, H. Tanaka, *Nat. Mater.* **2011**, *10*, 303.
[12] S. Kawata, H.-B. Sun, T. Tanaka, K. Takada, *Nature* **2001**, *412*, 697.
[13] N. Vasilantonakis, K. Terzaki, I. Sakellari, V. Purlys, D. Gray, C. M. Soukoulis, M. Vamvakaki, M. Kafesaki, M. Farsari, *Adv. Mater.* **2012**, *24*, 1101.
[14] J. Fischer, G. von Freymann, M. Wegener, *Adv. Mater.* **2010**, *22*, 3578.
[15] M. Farsari, M. Vamvakaki, B. N. Chichkov, *J. Opt.* **2010**, *12*, 124001.
[16] P. Tayalia, C. R. Mendonca, T. Baldacchini, D. J. Mooney, E. Mazur, *Adv. Mater.* **2008**, *20*, 4494.
[17] A. Ovsianikov, J. Viertl, B. Chichkov, M. Oubaha, B. MacCraith, I. Sakellari, A. Giakoumaki, D. Gray, M. Vamvakaki, M. Farsari, C. Fotakis, *ACS Nano* **2008**, *2*, 2257.
[18] M. T. Raimondi, S. M. Eaton, M. Laganà, V. Aprile, M. M. Nava, G. Cerullo, R. Osellame, *Acta Biomater.* **2013**, *9*, 4579.
[19] L. Amato, Y. Gu, N. Bellini, S. M. Eaton, G. Cerullo, R. Osellame, *Lab Chip* **2012**, *12*, 1135.